TECHNISCHE MECHANIK, 32, 2-5, (2012), 195 – 204
submitted: November 14, 2011

Image Correlation-Based Identification of Fracture Parameters for Structural Adhesives

R. Fedele, S. Sessa, N. Valoroso

We consider the identification problem of a cohesive model using kinematic full-field data obtained via digital image correlation during the fracture test of an adhesive joint. A criterion is presented for selecting measurements that exhibit optimal features for identification purposes. The proposed selection scheme is constructed using the sensitivity information and its performances are evaluated at varying noise-to-signal ratio.

1 Introduction

The development of high-strength structural adhesives has created many new uses for adhesive joints and established a need for additional theoretical and experimental investigation. Usually joints fail in the adhesive and, for an assembly that is properly designed, failure takes place *within* the adhesive layer (cohesive failure) rather than at the adhesive-substrate boundary. Predicting the behaviour of an adhesive joint is in general not an easy task due to a number of uncertainties concerning the assumed stress distribution, magnitude and direction of applied loads as well as changes in properties of adhesives during their service life. Because of that, design codes usually prescribe higher safety factors according to the importance of applications. Joints may be loaded to failure in the design configurations or in the form of test specimens and it is important to understand the response obtained by such testing especially for the apparently simple configurations used in international standards, that can be conveniently employed for data reduction. This is indeed a crucial point for design since the availability of material parameters from experiments and the general coherence between the data reduction schemes and the numerical model in which such parameters are used have a direct impact on the results of computations.

In this paper reference is made to a cohesive-zone model suitable to describe the nonlinear mechanical response of adhesively bonded assemblies originally developed by Valoroso and Champaney (2006). For the identification of the model parameters a global approach is adopted, in which the entire sample is modeled, as an alternative to the local methodology presented by Fedele et al. (2009) where only a small part of the specimen surface was accounted for. In particular, the data set for identification can be obtained via a Digital Image Correlation (DIC) procedure, which provides at different instants during the experiment kinematic full-field measurements on the free surface of the tested samples (Roux and Hild, 2008; Sutton et al., 2009). The main ingredients of DIC are summarized in Figure 1 that refers to a Double Cantilever Beam (DCB) test monitored by a digital camera, namely: (i) the reference (undeformed) image, with a pixel size of 19.5 μm, (ii) the finite element grid used for image correlation (element size is 12 pixel), and (iii) the reconstructed vertical displacement field.

The quantity and quality of experimental data obtained using DIC have to be carefully analysed. Actually, on one side, especially in presence of large noise-to-signal ratio, the overall information turns out to be smeared over a large number of data. On the other hand, a large set of noisy data with low sensitivities may contribute negatively to the identification process, see, e.g., Bolzon et al. (2002), and, in the most favorable scenario, they unnecessarily increase the problem size. In both cases, due to the accumulation of non-resolved residuals, uncertainty of kinematic measurements provided by DIC tends to increase with the number of processed digital images. Differently from Valoroso and Fedele (2010), the information provided by sensitivity maps in this study are exploited in order to formulate a selection criterion for extracting the optimal measurable quantities for identification purposes.

The paper is organized as follows. The constitutive model and the forward problem are presented in Section 2. The inverse identification problem and the sensitivity analysis based on the direct differentiation method are then recalled in Section 3. A selection criterion based on sensitivity maps is then presented in Section 4. The discussion of results is outlined in Section 5 and concluding remarks are given in Section 6.

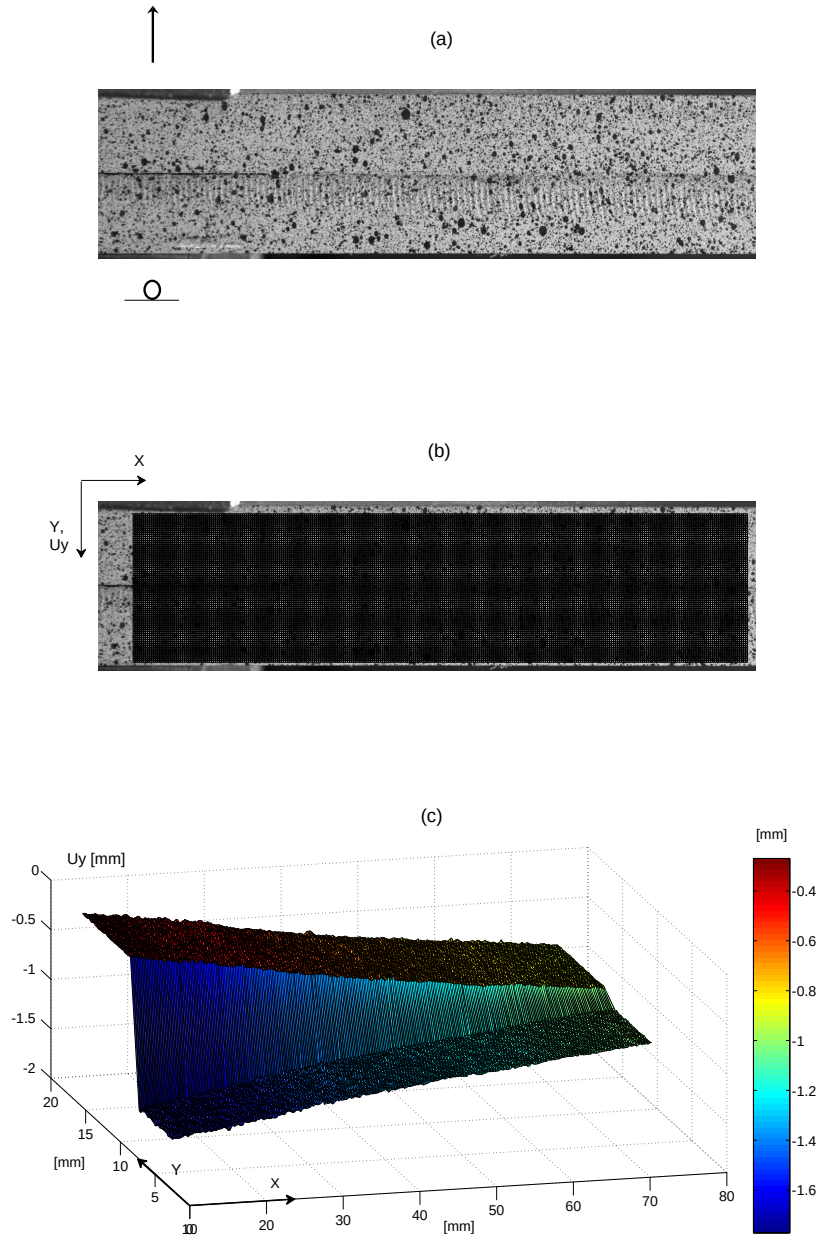

Figure 1: Symmetric DCB test. (a) Reference image (b) Finite element discretization for Digital Image Correlation (c) Reconstructed vertical displacement field. The inverted coordinates system is due to the imaging process.

2 Mechanical Model and Problem Set-Up

In this study reference is made to the one-dimensional (mode-I) version of the interface damage model proposed by Valoroso and Champaney (2006) and summarized in the following. The constitutive equations for the interface (normal) traction t and the damage-driving force Y are

$$\begin{aligned} t &= (1-D)k\langle[\![u]\!]\rangle_+ + k^-\langle[\![u]\!]\rangle_- \\ Y &= \frac{1}{2}k\langle[\![u]\!]\rangle_+^2 \end{aligned} \tag{1}$$

where $[\![u]\!]$ is the displacement discontinuity in the direction normal to the interface, $D \in [0,1]$ is the scalar damage variable and $\langle\cdot\rangle_\pm$ the positive (negative) part of the argument; symbols k and k^- denote in turn undamaged interface stiffnesses in tension and compression, the latter being understood as a penalty stiffness that enforces non-interpenetrability.

The damage law can be specified by prescribing that the force Y is bounded by a suitable threshold value $\bar{Y}$

$$\bar{Y} = \begin{cases} \displaystyle\int_0^\tau \dot{\bar{Y}}\, \mathrm{d}\tau = F(D) & \text{if } D \in [0,1[\\ \displaystyle\max_{\tau\in[0,T]} Y(\tau) & \text{if } D = 1 \end{cases} \tag{2}$$

and using the unilateral conditions

$$Y - \bar{Y}(D) \leq 0; \qquad \dot{D} \geq 0; \qquad \dot{D}\left(Y - \bar{Y}(D)\right) = 0 \tag{3}$$

to get damage irreversibility. The damage evolution is obtained by specifying the scalar function F in Eq. (2) as a monotonically increasing positive function of the argument D, see Valoroso and Champaney (2006) for a detailed account. In particular, the mode-I version of the interface model governed by an exponential traction-separation relationship, see also Figure 2, is obtained using

$$F(D) = -G_c \log(1 - D) \tag{4}$$

where $G_c \geq 0$ is the critical strain energy release rate, i.e. the total work of separation.

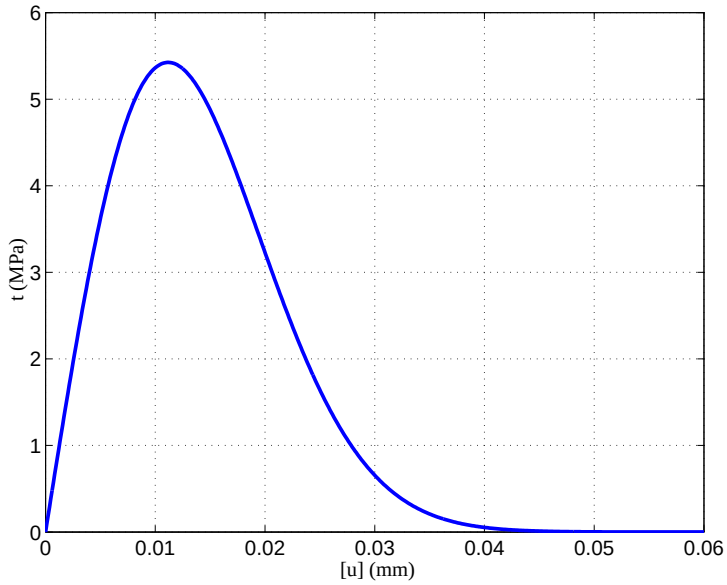

Figure 2: Mode-I cohesive relationship between normal traction t and displacement jump $\langle [\![u]\!] \rangle_+$ locally at the interface, generated by the target parameters $\overline{k} = 800$ [N/mm^3] and $\overline{G_c} = 0.1$ [N/mm].

In the present formulation the computation of the damage state only amounts to one function evaluation, since for damage loading ($\dot{D} > 0$) the value of the energy threshold $\bar{Y}$ equals that of the damage energy release rate Y. Accordingly, at each time τ the damage variable can be obtained from

$$D(\tau) = \min\left(1, \max_{(\rho \leq \tau)} \{F^{-1}(Y(\rho))\}\right) \tag{5}$$

The above described model depends on two material parameters collected in the vector $\boldsymbol{x}$:

$$\boldsymbol{x} = \begin{bmatrix} k \\ G_c \end{bmatrix} \tag{6}$$

that will be identified on the basis of the conventional symmetric DCB test.

The geometry of the test considered in our computations is shown in Figure 3; the left-end of the structure (intact part) is free, whilst on the right side two supports are prescribed and an increasing vertical displacement is imposed at the end of the upper arm. The nonlinear response of the DCB during the debonding tests is described using the damage model discussed in this section, which is taken as the constitutive law for zero-thickness interface elements that have been implemented as a part of a customized version of the FE code FEAP, Taylor (2009). As usual, the adherends are assumed to behave linearly elastically throughout the test that is simulated using plane strain conditions.

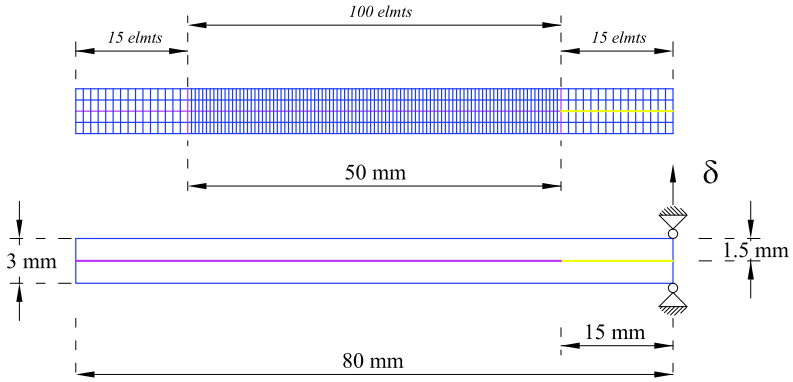

Figure 3: DCB test specimen. Geometry and finite element discretization.

3 Inverse problem and Sensitivity Maps

The relationship between the computed response $\boldsymbol{u}^{comp}$ (herein displacements) and the model parameters $\boldsymbol{x}$, usually referred to as forward (or direct) operator, is denoted as:

$$\boldsymbol{u}^{comp} = \mathbb{H}(\boldsymbol{x}) \tag{7}$$

The optimal parameters $\hat{\boldsymbol{x}}$ are then obtained as a solution of a nonlinear programming problem in which an objective function ω is minimized, see Tarantola (1987). Such function quantifies the discrepancy between the measured quantities $\boldsymbol{u}^{meas}$ at all considered instants and those computed as in Eq. (7) via the mathematical model as a function of the unknown parameters $\boldsymbol{x}$. The data set of the identification process is a time-space sampling of displacement components; in particular, the data vector $\boldsymbol{u}^{meas}$ will be constructed as a $n_y = (n_\tau \times n_u)$-dimensional vector containing the n_u nodal displacements selected at each measurement instant i ($i = 1\,, \ldots\,, n_\tau$). Such data can be provided by a DIC procedure concerning the deformation process of a suitable Region of Interest (ROI) that is monitored during the test (Fedele et al., 2009).

With this notation the inverse identification problem can be stated as follows:

$$\hat{\boldsymbol{x}} = \arg\min_{\boldsymbol{x}} \, \omega(\boldsymbol{x}) \tag{8}$$

with $\omega(\boldsymbol{x})$ the objective function

$$\omega(\boldsymbol{x}) = \left|\left| \mathbf{S} \cdot \left(\boldsymbol{u}^{meas} - \boldsymbol{u}^{comp}(\boldsymbol{x})\right) \right|\right|^2_{\mathbf{W}} \tag{9}$$

where the (squared) $\mathbf{W}$-norm is defined as

$$\left\|\boldsymbol{u}\right\|^2_{\mathbf{W}} = \mathbf{W}\boldsymbol{u} \cdot \boldsymbol{u} \tag{10}$$

and $\mathbf{W}$ is a diagonal matrix used for data scaling while $\mathbf{S}$ denotes a selection (Boolean) diagonal matrix, i.e. whose entries are either 0 or 1, acting as a mask on the vector of all measurable quantities. The error covariance matrix at the solution point is given by

$$\widehat{\mathbf{C}}_{\boldsymbol{x}} = \left(\mathbf{L}^T(\hat{\boldsymbol{x}})\, \widehat{\mathbf{C}}_u^{-1} \mathbf{L}(\hat{\boldsymbol{x}}) \right)^{-1} \tag{11}$$

where $\widehat{\mathbf{C}}_u$ is the (estimated) covariance matrix of the selected displacements

$$\widehat{\mathbf{C}}_u^{-1} = \widehat{\sigma}_u^{-2}\, \mathbf{I} \tag{12}$$

$\widehat{\sigma}_u$ is the standard deviation of the data set, and

$$\mathbf{L}(\boldsymbol{x}) = \frac{\partial \boldsymbol{u}}{\partial \boldsymbol{x}} \tag{13}$$

the corresponding sensitivity, the superscript $(\cdot)^{comp}$ being omitted for notational simplicity. It is worth emphasizing that: i) the simplifying assumption of un-correlated measurements, implying a diagonal form for the noise

covariance matrix in Eq. (12), turns out to be in safety favor since it corresponds to the worst scenario for identification without cross information between data; ii) Equation (11) is derived from the Markov' formula in presence of an indefinitely uncertain (Bayesian) a priori information, by linearizing the forward operator $\mathbb{H}(\boldsymbol{x})$ in the neighborhood of the solution point $\hat{\boldsymbol{x}}$.

Derivatives of the computed displacement field $\boldsymbol{u}$ with respect to the material parameters to identify are a key ingredient of the present identification procedure. Actually, the sensitivity information is needed both for the optimal design of the experiments, and to compute gradients required in the first-order minimization procedure. The method adopted here for sensitivity computations is based on the Direct Differentiation of the governing equations, and has been implemented in the same FE code employed for forward simulations. A detailed discussion on this topic is outside the scope of this work and can be found elsewhere, see, e.g., Kleiber et al. (1997). We here limit ourselves to recall that the displacement sensitivities can be obtained from the finite element residual equations at the k-th loading step

$$\mathbf{R}^{(k)} = \mathbf{R}(\boldsymbol{u}^{(k)}(\boldsymbol{x}), \boldsymbol{x}) = \mathbf{0} \tag{14}$$

via linearization with respect to the material parameters to get:

$$-\frac{\partial \mathbf{R}^{(k)}}{\partial \boldsymbol{u}} \quad \left[\frac{\partial \boldsymbol{u}^{(k)}}{\partial \boldsymbol{x}}\right] = \left[\frac{\partial \mathbf{R}^{(k)}}{\partial \boldsymbol{x}}\right] \tag{15}$$

In closing this section we recall that the computation of displacement sensitivities requires a little extra computing time since the coefficient matrix for the above equation is the usual FE tangent matrix and that, for the DCB problem at hand, the only non-zero contributions to the pseudo-load vector $\frac{\partial \mathbf{R}^{(k)}}{\partial \boldsymbol{x}}$ come from interface elements since the adherends are linearly elastic. It is also worth noting that the same equation for sensitivity computations also holds for nonlinear elasticity or holonomic elastic-plastic behaviour.

4 Space-Time Sampling of Measurable Quantities

In the following a selection criterion based on sensitivity maps is presented for the identification of mode-I cohesive parameters resting on kinematic full-field data. Such criterion allows one to perform the space and time sampling of the available nodal displacements that can be obtained via DIC, and then will specify the entries of Boolean matrix $\mathbf{S}$ multiplying the data vector in Equation (9), to be 1 if the relevant datum is retained for identification, and 0 if not. The selection criterion is defined by a condition such as:

$$g(u_v) = .TRUE. \qquad \Rightarrow \qquad \mathbf{S}_v = 1 \tag{16}$$

being g a logical variable and v a set of indices relevant to the selected displacement components u.

Let P be a generic node of the adopted space discretization; at each time station τ_m, let us consider the spatial distribution of sensitivities within the ROI, namely the derivatives of a displacement component u_i with respect to a model parameter x_j, being here $i, j \in \{1, 2\}$. The following thresholds can be defined:

$$l_{ij} = \max_{P \in \mathrm{ROI}} \left(\max_{m=1,\ldots,n_\tau} \left| \frac{\partial u_i}{\partial x_j}(P, \tau_m) \right| \right) \tag{17}$$

The inner maximization in Eq. (17) is performed in time, separately for each node P, i.e. the node location is frozen. Thereafter, the outer maximization allows one to compare performance of different nodes inside the ROI. It is worth noting that Equation (17) disregards any time-dependence of the threshold. According to this criterion, a single displacement component at node Q and time station τ_m, $u_i(Q, \tau_m)$, is selected for the identification process and included in the objective function ω, if the following condition is met (different for $i = 1$ or $i = 2$):

$$\tau = \tau_m \,,\, i = 1, 2 \qquad g_i = \bigcup_{j=1,2} \quad \left\{ \left| \frac{\partial u_i}{\partial x_j}(Q, \tau_m) \right| \geq s \cdot l_{ij} \right\} \tag{18}$$

Symbol $\bigcup$ denotes the logical operator OR, implying selection if at least one of the two inequalities in Eq. (18) is satisfied, concerning derivatives of the same displacement component with respect to the model parameter $x_j, j \in \{1, 2\}$. In Eq. (18) the scalar coefficient $s \in [0, 1]$ allows the user to relax continuously the optimality thresholds. For the sake of simplicity the same s is assumed for all the coefficients l_{ij}. For $s = 0$, all the available nodal displacements trivially satisfy Eq. (18) and they are all processed for identification. Obviously, for $s = 1$ at least one displacement component is included in the objective function to minimize (along with other

components at the same time station τ_m equally sensitive, if any). It may also occur that, at a given time station τ_m, no displacement components are selected, since they turn out to be not sufficiently sensitive to the interface parameters. Anyway, both horizontal and vertical displacement components are selected, since distinct thresholds are adopted for them. The proposed criterion in Eq. (18) is quite general and can be effectively applied even in presence of plastic dissipation within the metal adherends. Moreover, it includes as a particular case also selection criteria possibly based on Linear Elastic Fracture Mechanics (LEFM), namely derived under the assumption of linear elastic response of the adherends. For instance, one could reasonably expect that the most sensitive measurements at each instant of the test are located in a neighborhood of the crack tip, and therefore, in a weighted least square approach, they could be given a weight proportional to $(1/r)$, being r the radial distance from the current crack tip. Actually, the dependence of displacement sensitivities on $1/r$ is fully caught by the discretized version of a Green-like function, namely some properly defined elastic influence matrix $\mathbf{G}$, based on the relationship (see Bolzon et al., 2002):

$$\frac{\partial \mathbf{u}}{\partial \mathbf{x}} = \mathbf{G} \cdot \frac{\partial \mathbf{\Delta}}{\partial \mathbf{x}} \tag{19}$$

where vector $\mathbf{\Delta}$ collects the displacement discontinuities at the interface nodes, i.e. the discretized counterpart of quantities $[\![u]\!]$ in Eq. (1).

In order to compare a posteriori the information content of the selected data set, a strategy suitable to deal with the fundamental tradeoff between bias and variance is introduced. To this purpose, let us consider the following confidence ellipsoid in the n_x-dimensional space of model parameters $\boldsymbol{x}$:

$$\mathbb{E}_{1-\alpha} = \left|\left|\boldsymbol{x} - \hat{\boldsymbol{x}}\right|\right|^2_{\widehat{\mathbf{C}}_{\boldsymbol{x}}^{-1}} - \chi^2_{1-\alpha,\, n_x-1} = 0 \tag{20}$$

where symbol $\chi^2_{1-\alpha,\, n_x-1}$ denotes the upper $(1-\alpha)$-quantile of the Chi-square probability density distribution with $(n_x - 1)$ degrees of freedom. The estimated mean value vector $\hat{\boldsymbol{x}}$ obtained from the identification process represents the center of the ellipsoid, and the quadratic form is associated to the covariance matrix of the estimation error $\widehat{\mathbf{C}}_{\boldsymbol{x}}$, given as in Equation (11). Under the hypothesis of Gaussian distribution for vector $\boldsymbol{x}$, the true parameter vector (n_x-dimensional) is expected to belong to the ellipsoid Eq. (20) with a probability of $1-\alpha$. In the following reference is made to the confidence ellipse in Eq. (20) with $\alpha = 0.05$ meaningful from an engineering standpoint, denoted in what follows by symbol $\mathbb{E}_{0.95}$. It is well-known that the square lengths of the principal diameters of the ellipsoid equal the eigenvalues of the current covariance matrix $\widehat{\mathbf{C}}_{\boldsymbol{x}}$ and that the volume bounded by the ellipsoid is proportional to the product of the lengths of the principal axes, i.e. to the determinant of $\widehat{\mathbf{C}}_{\boldsymbol{x}}$. These geometric properties allow one to graphically visualize the confidence level of the estimates and the effectiveness of the identification procedure, see e.g. Tarantola (1987). However, from an engineering standpoint there is a special need for a scalar performance index, to be dealt with easily. To this purpose, the constrained nonlinear programming problem is considered:

$$\boldsymbol{x}^* = \arg\max_{\boldsymbol{x}} \left\{ \left\| \boldsymbol{x} - \overline{\boldsymbol{x}} \right\| \quad | \quad \boldsymbol{x} \in \mathbb{E}_{0.95} \right\} \tag{21}$$

with $\|\cdot\|$ the usual Euclidean norm. Vector $\boldsymbol{x}^*$ represents the point belonging to the $(1-\alpha)$-confidence ellipsoid which is the farthest from the target parameter vector $\overline{\boldsymbol{x}}$, which is known a priori since pseudo-experimental data are considered for the validation of the procedure. Therefore, the distance:

$$\mathrm{d}_{0.95} = \left\| \boldsymbol{x}^* - \overline{\boldsymbol{x}} \right\| \tag{22}$$

depends both on the location of the estimated parameters vector with respect to the correct parameter vector $\overline{\boldsymbol{x}}$, and on the estimated covariance matrix (i.e. on both its axes and their orientation). Using the parametric representation of the ellipsoid, the problem defined by Eq. (21) is equivalent to a $(n_x - 1)$-dimensional search, the maximisation being performed in the definition domain of the bijective map $\boldsymbol{x} = \boldsymbol{x}(q)$. Herein $n_x = 2$, i.e., the confidence domain is bounded by an ellipse, and $q \in [0, 2\pi]$ is a scalar parameter. The error distance Eq. (22) can be computed in the space of normalized parameters $x_j/\overline{x}_j$, with a suitably scaled covariance matrix.

It is worth emphasizing what follows.

i) The error distance Eq. (22) allows one to quantify a posteriori the information content of a given data set with reference to a specific model and parametrization.

ii) The above distance does not vanish if the bias is null, i.e. if the parameter vector is estimated correctly and $\hat{\boldsymbol{x}} \to \overline{\boldsymbol{x}}$, since the relevant covariance matrix may be different from zero. On the contrary, the above distance is null when also the error covariances vanishes, i.e. $\widehat{\mathbf{C}}_{\boldsymbol{x}} \to \mathbf{0}$.

iii) The proposed error distance allows one to easily compare the quality of identification results taking into account both the mean value vector and the covariance matrix.

5 Results and Discussion

The results presented in this section refer to a DCB specimen whose size and geometry are shown in Figure 3. The finite element model has been developed in a customized version of the FEAP code (Taylor, 2009). The simulation is performed under displacement control and the adopted discretization consists of 520 enhanced assumed strain elements for the bulk material and 115 zero-thickness interface elements along the joint. To generate *pseudo-experimental* data, i.e. synthetic data for the validation stage, the mechanical response of properly designed aluminum adherends is assumed to be linearly elastic, with $E = 72.0\,\mathrm{GPa}$, $\nu = 0.3$, and the cohesive parameters object of the identification procedure are taken as:

$$\overline{\boldsymbol{x}} = \left[\begin{array}{c} \overline{k} \\ \overline{G}_c \end{array} \right] = \left[\begin{array}{c} 800\ \mathrm{N/mm^3} \\ 0.1\ \mathrm{N/mm} \end{array} \right] \tag{23}$$

At each time station τ_m, $m = 1, ..., n_\tau \equiv 400$, displacements (amounting to $n_u = 1,570$) endowed by parameter sensitivities are provided by the FE code to the minimization algorithm, developed in a Matlab environment (The MathWorks, 2009). The overall number of kinematic data here available amounts to $n_y = 628,000$. To simulate the scatter of experimental measurements, synthetic data have been corrupted by an additive Gaussian noise with null mean and increasing standard deviation $\widehat{\sigma} = 1\,,\, 10\,,\, 50\,,\, 100$ μm kept constant during the test. The stability of the inverse procedure can be assessed by comparing the resulting estimates to the correct values $\overline{k}$ and $\overline{G}_c$ which are known a priori. It is worth noting that, for the problem at hand, the considered range of noise is extremely wide. In fact, uncertainty related to kinematic full-field measurements provided by 2D-DIC usually amounts to about $1/10 \div 1/20$ of the pixel size, depending on the surface texture and image quality. Using a standard digital camera with a 16 Megapixel sensor, a large part of the sample surface lies inside the field-of-view, the estimated pixel size amounts to about 20 μm, and in the worst scenario the uncertainty on reconstructed displacement should not exceed $1 \div 2$ μm, as it can be envisaged in Figure 1-(c). Once that Boolean matrix $\mathbf{S}$ has been specified, minimization of the objective function $\omega(\boldsymbol{x})$ in Eq. (9) is performed through a two-step strategy: first, a zero-order, direct-search simplex algorithm; ii) thereafter, a first-order gradient-based, interior-point trust region algorithm, suitable for large-scale problems. The former is suitable to deal with the possible presence of local minima, and the latter is employed when the current estimates are definitely in the neighborhood of the minimum.

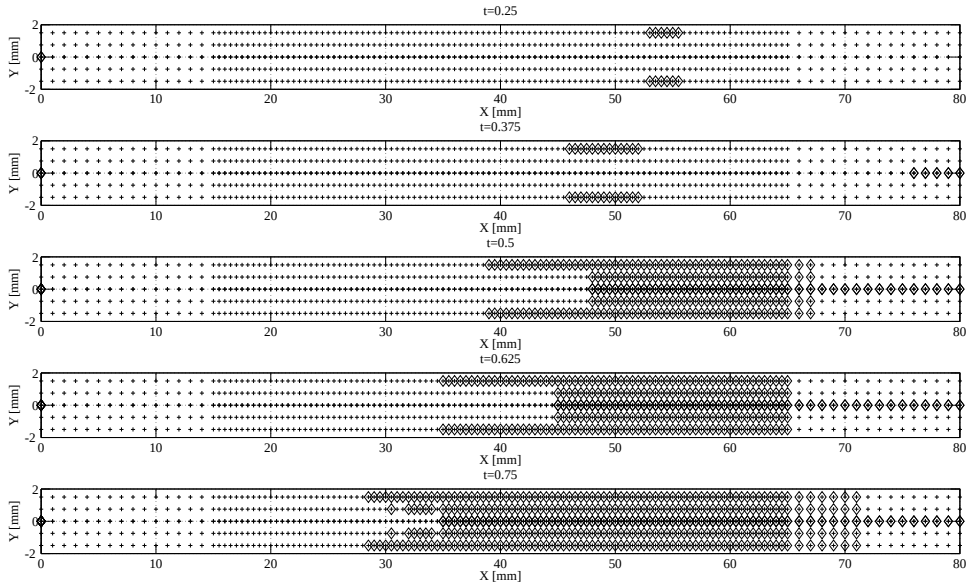

Figure 4: Data sampling with threshold coefficient $s = 0.3$. Node locations are evidenced by symbol $+$; nodes selected by the proposed strategy at different instants are marked by rhombs.

The selection performed by the proposed criterion is sketched in Figure 4, where the nodes of the adopted finite element discretization are identified by a plus symbol, and nodes at which a displacement component is retained for identification are highlighted by rhombs. Performance index in Eq. (22) is shown in Figure 5 as a function of the number of data processed. It can be noticed that the error distance stabilizes starting from a critical size of sampled data, which exhibits also a small dependence on the level of data noise. As expected, an increase of noise level yields higher estimation errors: this fact can be easily recognized since, at least for the considered exercises, plots relevant to different noise levels do not intersect each other. Therefore, any increase of the sample size besides the *critical* one, turns out to be useless for identification purposes. The error $d_{0.95}$ resulting for samples size exceeding the *critical* one, can be regarded as an *asymptotic* error, since it can be achieved rigorously when $n_y \to \infty$. As expected, such error distance increases with the intensity of data noise. On the basis of these preliminary results, it clearly appears that the number of kinematic measurements required to achieve accurate parameter estimates turns out to be quite large compared to conventional data used for parameter identification, see e.g. Bolzon et al. (2002). In particular, for all considered noise levels, the proposed selection criterion exhibits excellent performances also for a narrow data set, namely less than $15,000$.

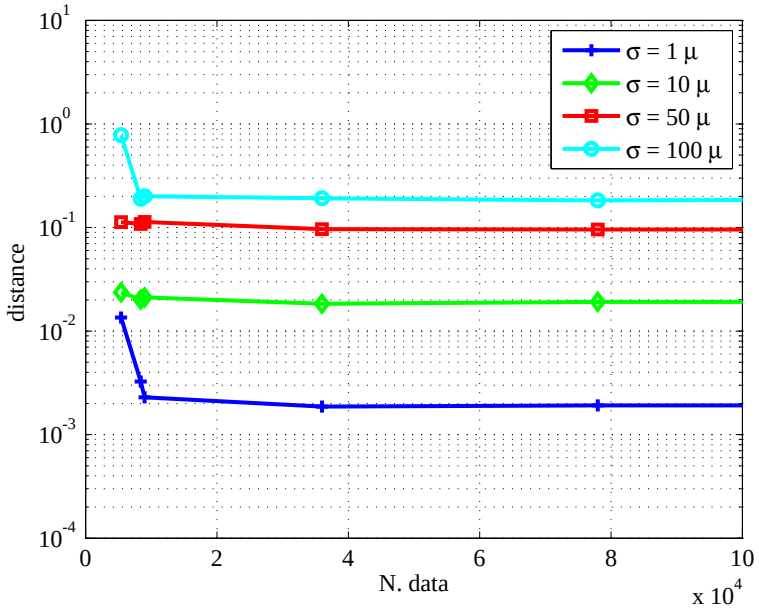

Figure 5: Error distance $d_{0.95}$ vs number of processed data, by increasing the noise standard deviation $\widehat{\sigma}$.

Figure 6 shows the error ellipses $\mathbb{E}_{0.95}$ defined by Eq. (20) as a function of the processed data set, at varying threshold coefficient s. It can be noted that, for a low noise level ($\sigma = 1\,\mu$m in Fig. 6-a), the ellipse axes exhibit comparable lengths, since in this case the estimation uncertainties concerning the two parameters are of the same magnitude. On the contrary, for higher noise ($\sigma = 100\,\mu$m in Figure 6-b) the differences in the estimation of the two parameters become more significant, and the area delimited by the ellipses is now significantly larger than in the previous case. As the size of processed data increases, the centers of the ellipses, represented by the parameter mean value estimates, translate towards the solution point, whilst the directions and lengths of the principal axes change. As expected, in presence of a severe noise level, the normalised uncertainty related to parameter G_c turns out to be at least two orders of magnitude lower than the one relevant to parameter k. Actually, as already discussed in Valoroso and Fedele (2010), parameter G_c represents in a sense an integral measure of the interface relationship since it represents the energy required to form a new traction-free surface of unit area, whilst the tangent stiffness at the origin k, governing the local shape of the cohesive law, has to be regarded as a more localized property in that it only affects the local stress distribution within the cohesive zone but not the local stress resultant.

6 Concluding Remarks

In order to get effective simulations up to failure of adhesively bonded assemblies, rigorous calibration procedures should be adopted, based on accurate measurements of local damage phenomena. Nowadays no-contact, full-field techniques make available an enormous quantity of data. When dealing with such huge information, two alternatives can be envisaged:

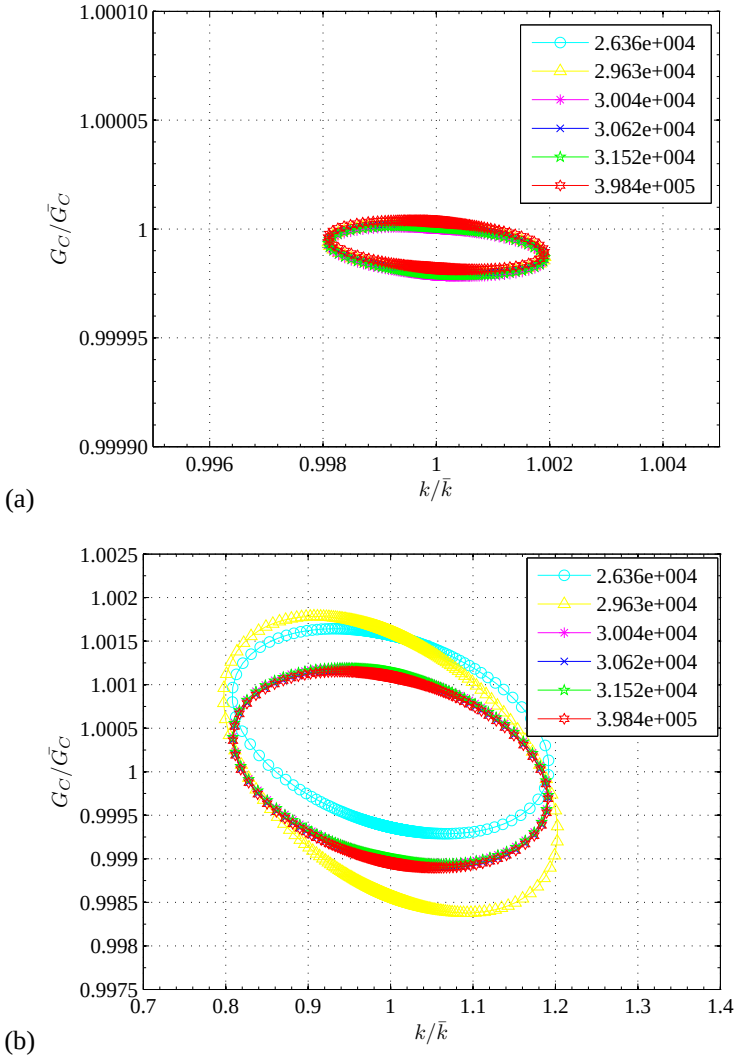

Figure 6: Error ellipses in the normalised parameter space as a function of the processed sample size (at varying threshold coefficient s). Standard deviation of data noise equal to: (a) $\sigma = 1$ μm and (b) $\sigma = 100$ μm.

i) use of suitable technical solutions capable of dealing with large amounts of data simultaneously and at high speed;

ii) implementation of strategies for data selection, in order to discard those information that are either redundant or irrelevant for the identification process.

In this paper a criterion has been presented for selecting, within the set of kinematic measurements obtained during a mode-I debonding test, data with the highest information content for identification purposes. The proposed criterion relies upon sensitivity maps, which can be made available at a negligible computational cost by implementing the direct differentiation method in the same finite element code used for forward analyses. It is worth emphasizing that such criterion can be applied also in the presence of nonlinear behaviour of the metal adherends, and therefore the present approach turns out to be more general with respect to other strategies apparently more intuitive based upon LEFM concepts. Data samples with the same size but selected according to different criteria, herein not documented for brevity, can lead to identification results markedly different; this circumstance motivates the search for an optimal selection strategy. In particular, the results presented in this paper show that, in presence of relatively small data sets, the quality of identification cannot be derived exclusively on the basis of the processed sample size and of the noise standard deviation $\widehat{\sigma}$, but it can better assessed using as additional information their sensitivity distribution in space and time. Only when the number n_y of processed data is very large, i.e. mathematically for $n_y \to \infty$ and practically some hundreds of thousands data for the problem in point, the actual distribution of parameter sensitivities plays a negligible role and the quality of processed data for identification can be satisfactorily described by average features, such as their global number and uniform standard deviation.

In conclusion, the main results of the present study can be summarized as follows. The minimum number of data required to achieve a satisfactory estimation of the model parameters, i.e. with errors close in percentage to the *asymptotic* values, strongly depends on the noise level. Actually, when the standard deviation of white noise is increased, one needs data samples progressively wider in order to achieve the stabilization. This circumstance appears to have a sound basis, since in presence of high noise levels the information are typically atomized over the entire data set, so that each datum possesses only a small part of it. Furthermore, the estimation accuracy strongly depends from the adopted selection criterion, namely the quality of estimates based on data samples with an identical size can vary markedly depending on the adopted selection strategy. In particular, on the basis of the identification exercises carried out by the authors, the selection criterion presented in the paper exhibits good performances also in presence of relatively small data samples.

The present study represents a contribution for defining a road map to follow in order to increase the robustness of identification procedures without necessarily increasing the number of processed data. When one expands the number of kinematic data, which is directly related to the number of digital images to be analyzed, both the computational cost of the image correlation procedure and the uncertainty relevant to the reconstructed displacement fields are expected to increase. Unlike the number of acquired images, which is controllable, their space resolution depends by the adopted digital sensor on one hand and on the natural or artificial surface texture of the monitored specimens on the other one. And these factors cannot be arbitrarily varied by the user.

Acknowledgements

This research has been carried out as part of the project *Analysis of structural adhesive joints. Modelling and experimental testing via DIC*, within the MiSE-ICE-CRUI 2008 research program. The financial support of the Italian Ministry of Economic Development (MISE) and the Italian Institute for Foreign Trade (ICE) is gratefully acknowledged.

References

Bolzon, G.; Fedele, R.; Maier, G.: Parameter identification of a cohesive crack model by Kalman filter. *Computer Methods in Applied Mechanics and Engineering*, 191, 25-26, (2002), 2847–2871.

Fedele, R.; Raka, B.; Hild, F.; Roux, S.: Identification of adhesive properties in GLARE assemblies using digital image correlation. *Journal of the Mechanics and Physics of Solids*, 57, 7, (2009), 1003–1016.

Kleiber, M.; Antúnez, H.; Hien, T.; Kowalczyk, P.: *Parameter Sensitivity in Nonlinear Mechanics. Theory and Finite Element Computations*. John Wiley & Sons Ltd, Chichester, UK (1997).

Roux, S.; Hild, F.: Digital Image Mechanical Identification (DIMI). *Experimental Mechanics*, 48, (2008), 495–508.

Sutton, M.; Orteu, J. J.; Schreier, H.: *Image correlation for shape motion and deformation measurements*. Springer-Verlag, Heidelberg (2009).

Tarantola, A.: *Inverse Problems Theory. Methods for Data Fitting and Model Parameter Estimation* (1987).

Taylor, R.: *FEAP - User and Programmer Manual*. University of California at Berkeley, *http://www.ce.berkeley.edu/∼rlt* (2009).

The MathWorks, I.: *Matlab 7.8, Optimization Toolbox 4.2 Manual* (2009).

Valoroso, N.; Champaney, L.: A damage-mechanics-based approach for modelling decohesion in adhesively bonded assemblies. *Engineering Fracture Mechanics*, 73, 18, (2006), 2774–2801.

Valoroso, N.; Fedele, R.: Characterization of a cohesive-zone model describing damage and de-cohesion at bonded interfaces. sensitivity analysis and mode-I parameter identification. *International Journal of Solids and Structures*, 47, 13, (2010), 1666–1677.

Addresses: Dr.-Ing. Roberto Fedele, Assistant Professor, and Dr.-Ing. Salvatore Sessa, post-Doc research associate, Politecnico di Milano, Dipartimento di Ingegneria Strutturale, P.zza Leonardo da Vinci 32, 20133 Milan (Italy). Prof. Dr.-Ing. Nunziante Valoroso, Università di Napoli Parthenope, Dipartimento per le Tecnologie, Centro Direzionale Isola C4, 80143 Napoli (Italy).
email: `fedele@stru.polimi.it; nunziante.valoroso@uniparthenope.it`